

Laser processing of ceramics of the $\text{SiO}_2\text{-Al}_2\text{O}_3$ system

Y. N. SHIEH, R. D. RAWLINGS, D. R. F. WEST

Department of Materials, Imperial College of Science, Technology and Medicine, London SW7 2BP, UK

An investigation has been made of the constitution of laser-processed ceramics from the $\text{SiO}_2\text{-Al}_2\text{O}_3$ system. Samples were produced in the form of pellets a few millimetres in diameter by pulsed laser melting of mixtures of silica and alumina powders containing 40, 60 and 70 mol% Al_2O_3 . X-ray diffraction identified the main crystalline phases as Al_2O_3 in the pellets produced from the 70 mol% Al_2O_3 mixture and mullite from the 60 and 40 mol% Al_2O_3 mixtures. The proportion of glassy phase present increased with increasing SiO_2 content. Microstructural observations on the 60 mol% Al_2O_3 pellet showed primary mullite crystals and a lamellar structure interpreted as a eutectic of Al_2O_3 and mullite. Pellets prepared by melting kaolin powder consisted essentially of a glassy phase and much porosity. Cladding of an alumina substrate, carried out using a continuous powder feed into a laser-generated melt pool, was carried out using the same silica-alumina mixtures as those employed for pellet production. A clad layer was also produced by preplacing a kaolin coat on the alumina substrate prior to laser processing. The effects of traverse speed over the range 3.7 to 7.4 mm s^{-1} inclusive, power density (44.4 and 111 W mm^{-2}) and powder flow rate (0.13 to 0.47 g s^{-1} inclusive) were investigated. It was found that the phases present in the clad layer depended on the composition of the precursor powder and the processing conditions. Microstructural examination of the clad layers produced from $\text{SiO}_2\text{-60 mol% Al}_2\text{O}_3$ and kaolin that had completely melted during processing exhibited various growth morphologies.

1. Introduction

The use of lasers in industrial applications has grown considerably over the last twenty years due to attractive features such as the provision of a high-intensity and clean source of energy, allowing non-contact processing and the capability of working over a wide range of power densities, thus making the processing of both low and high melting-point materials possible. Laser processing of metals has developed strongly over this period but there are few examples of industrial laser processing of ceramics; the only widespread application of lasers in ceramic processing is the cutting of thin sections, mainly for the electronics industry. There is also a relative dearth of fundamental information on the response of ceramics to a laser beam. A limited number of papers have been published on laser welding and cutting of ceramics [1-3], sealing of plasma-sprayed layers [4-6], cladding of ceramics on to metal [7-9], laser surface melting [10], alloying [11] and evaporation of ceramics [12].

The major drawbacks to laser processing of ceramics are cracking due to their poor thermal shock resistance and the lack of information on the structure and properties of solidified material, as ceramics are conventionally produced by solid-state routes. Thus, in spite of the inherent problem of thermal shock, it was considered opportune to institute a fundamental

study of melting, solidification and cladding using laser technology.

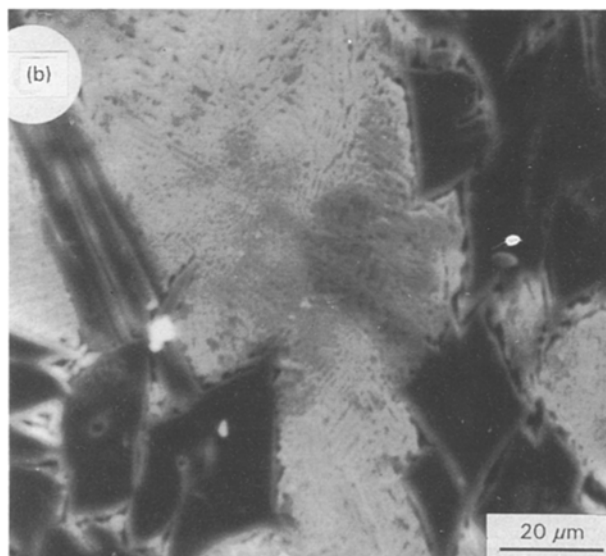
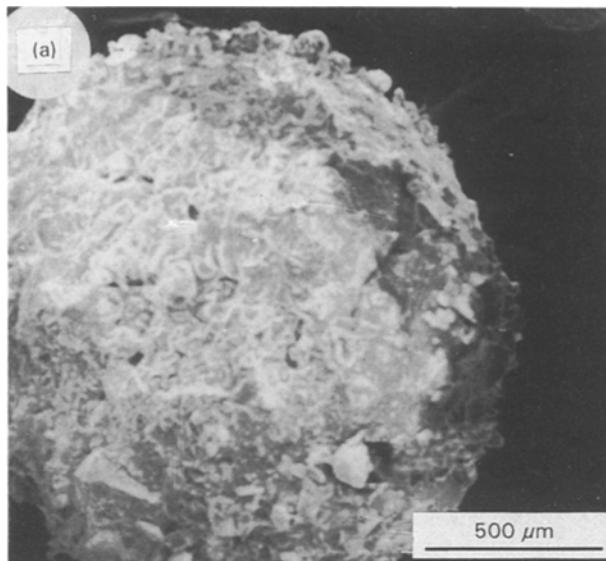
The work most relevant to the present investigation is that on laser surface alloying [11]. Alumina was precoated with either kaolin or a $\text{SiO}_2\text{-60 mol% Al}_2\text{O}_3$ mixture prior to processing at a laser power of 0.4 kW. The laser-processed surface layer so produced was glassy but could be crystallized, albeit slowly in the case of kaolin, by an appropriate high-temperature heat treatment. The work reported here is an extension of this investigation and was devised to explore in more detail the practicability of laser-processing ceramics, and in particular to study the structures produced by solidification at relatively high cooling rates in the $\text{SiO}_2\text{-Al}_2\text{O}_3$ system. Two laser-processing techniques have been employed, namely (a) the production of small pellets by pulsed laser melting of powders, and (b) cladding on a preheated Al_2O_3 substrate.

2. Experimental procedure

All the powders used in this study were obtained from BDH Chemicals. The SiO_2 was a silica acid-washed powder with irregular, angular-shaped particles mainly in the size range 75-110 μm . The alumina, Al_2O_3 , particles were approximately spherical agglomerates of 50-75 μm diameter consisting of much smaller

crystals. The kaolin was of nominal composition (wt %) 43.5% SiO₂, 36.5% Al₂O₃, 1.5% K₂O, other oxides 0.5% and the balance H₂O; the particles were small (< 10 μm) and tended to stick together, hence the powder did not flow well. The substrate used for the cladding experiments was Al₂O₃ of 98 wt % purity, the impurities being mainly SiO₂, CaO and MgO, and was supplied as 3 mm plate by Morgan Matroc Ltd, Stourport-on-Severn, UK.

The silica and alumina powders were mixed in a tumble roller overnight to give homogeneous mixtures of the following compositions (mol %): SiO₂-70% Al₂O₃, SiO₂-60% Al₂O₃ and SiO₂-40% Al₂O₃. Processing was carried out using a 1 kW CO₂ laser (Ferranti MFK1). For the production of pellets from the SiO₂-Al₂O₃ mixtures and from the kaolin, the powder was placed in a ceramic crucible (30 mm diameter and 10 mm deep) and a small volume melted by a pulsed laser beam fired for 0.5 s at 1 kW power. This produced solidified pellets of approximately spherical shape (Fig. 1a) and of 1–4 mm diameter. A similar method of processing has been previously used in investigations of the structure of rapidly solidified metallic alloys [13].



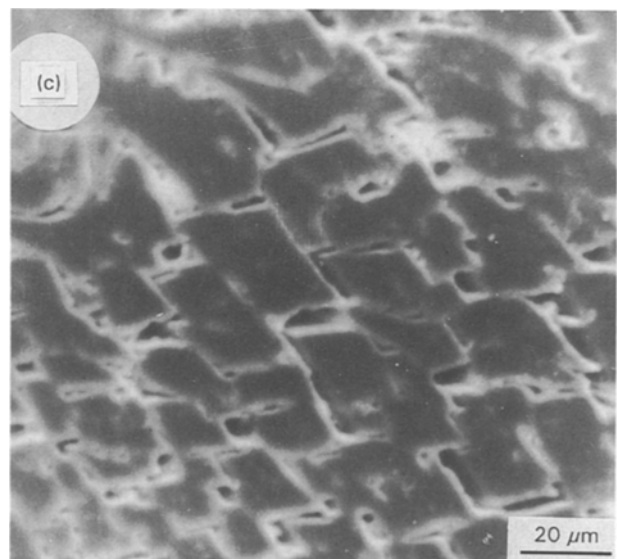
In the cladding process the three silica-alumina mixtures were each injected into the laser-generated melt pool by a continuous feed process, using argon carrier gas in a manner similar to that described in previous publications [8, 9]. The usual process parameters were beam diameter 3 mm, traverse speed 3 or 5 mm s⁻¹, power 1 kW (continuous wave, CW), powder feed rate 0.47 g s⁻¹ and substrate temperature 800 °C. To investigate the effects of processing conditions the SiO₂-60% Al₂O₃ mixture was processed at a range of powder flow rates (0.13 to 0.47 g s⁻¹ inclusive), two different power densities (44.4 and 111 W mm⁻²) and various traverse speeds (3.7 to 7.4 m s⁻¹ inclusive). When cladding with kaolin the powder was preplaced, using a modification of the method employed by Chaim *et al.* [10], since feeding was not satisfactory with the fine powder. The preplacing was achieved by coating the substrate with a thick kaolin slurry and drying prior to processing with beam diameter 4 mm, traverse speed 5 mm s⁻¹, power 1 kW (CW) and a 600 °C preheat temperature.

After laser processing the phases present were identified by X-ray diffraction (XRD) using CuK_α radiation and a graphite single-crystal monochromator. The pellets were ground to powder prior to examination. The clad layers were either removed from the substrate and ground to powder or, if well adhered to the substrate, polished flat and then examined.

Pellets and clad layers were sectioned, polished, etched and carbon- or gold-coated for determination of microstructures by scanning electron microscopy (SEM). Energy-dispersive analysis of X-rays (EDAX) was utilized for the measurement of composition in selected regions of the samples.

Microhardness tests were performed on a polished sample of the SiO₂-60 mol % Al₂O₃ precursor clad layer using a Leitz Miniload 2 diamond pyramid

Figure 1 Surface topography and microstructure of a pellet produced from the powder mixture SiO₂-60 mol % Al₂O₃: (a) surface of pellet with unmelted particles, (b) region with microstructure consisting of large angular primary crystals of mullite and a eutectic of mullite and alumina, (c) region with a microstructure mainly consisting of primary mullite crystals.



microhardness tester with a 500 g load. The mean of at least three indentations was used to obtain a microhardness value, except when a microhardness trace was made across the section of a sample in order to correlate microhardness with local changes in microstructure.

Differential thermal analysis (DTA) was carried out on selected powdered laser-processed samples to obtain information on the glass transition and the crystallization temperatures of any glass present. An alumina reference was used and the operating conditions were a heating rate of $20\text{ }^{\circ}\text{C min}^{-1}$ from room temperature up to $1400\text{ }^{\circ}\text{C}$ in an air atmosphere.

3. Results

3.1. Pellets

X-ray diffraction showed the presence of the phases listed in Table I. The indications of the proportions are only semi-quantitative.

Microstructural observations were only made on the pellets produced from SiO_2 -60% Al_2O_3 and kaolin powders. The SiO_2 -60% Al_2O_3 pellets consisted of relatively large ($\sim 20\text{ }\mu\text{m}$) angular crystals together with a lamellar two-phase structure of eutectic-like appearance (Fig. 1); a small proportion of featureless material, interpreted as a glassy phase, was also observed. Small particles typically $100\text{ }\mu\text{m}$ in size, apparently of unmelted SiO_2 powder, were seen on the pellet surface and would account for the small amount of SiO_2 detected by X-ray diffraction. The most notable feature of the kaolin pellets was the large amount of porosity, which varied in size and distribution from pellet to pellet and within a given pellet. For example, Fig. 2a shows a large $1000\text{ }\mu\text{m}$ pore and Fig. 2b a region in the same pellet with many pores of only $25\text{ }\mu\text{m}$. Crystalline phases were not clearly observed due to the small amount present, according to the X-ray data, and the complication of the large amount of porosity.

DTA of the pellets produced from kaolin showed the glass transition temperature to be about $700\text{ }^{\circ}\text{C}$. An exothermic peak, attributed to crystallization of the glass, was present at $973\text{ }^{\circ}\text{C}$. The X-ray data for a pellet heat treated for 1 h at $1100\text{ }^{\circ}\text{C}$ showed an increase in the proportion of mullite and a reduction in the diffuse halo, thus confirming that the exothermic peak was due to crystallization to mullite (Fig. 3).

TABLE I Phases detected and their proportions in the laser-processed pellets as determined by X-ray diffraction

Composition of powder (mol %)	Phase proportion			
	Mullite	Alumina	Silica	Glass
SiO_2 -40% Al_2O_3	Large	None	Small	Large
SiO_2 -60% Al_2O_3	Large	Medium	Very small	Small
SiO_2 -70% Al_2O_3	Large	Large	Very small	Very small
Kaolin	Small	None	None	Large
Kaolin (HT ^a at $1100\text{ }^{\circ}\text{C}$)	Substantial	None	None	Significant

^aHeat-treated after laser processing.

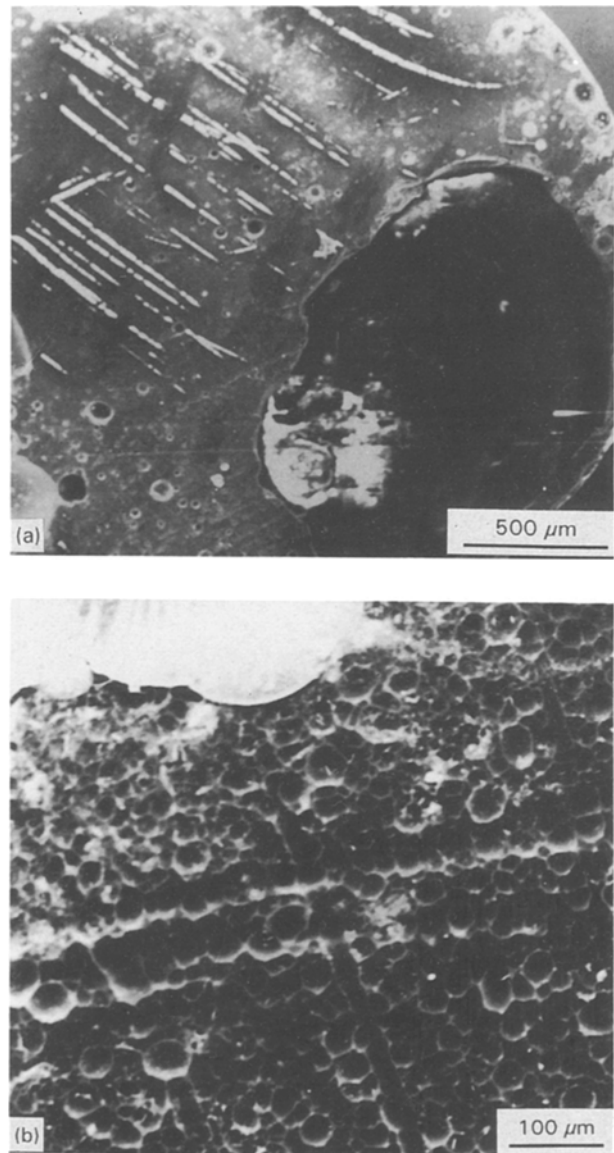


Figure 2 Microstructure of a pellet produced from kaolin powder: (a) region with a large pore, (b) region with many small ($\sim 25\text{ }\mu\text{m}$) pores.

3.2. Clad layers

The profile of a clad layer produced using SiO_2 -60% Al_2O_3 mixture at a powder feed rate of 0.47 g s^{-1} , beam diameter 3 mm , traverse speed 5 mm s^{-1} and substrate preheat temperature $800\text{ }^{\circ}\text{C}$ is given in Fig. 4. It can be seen that the track is asymmetrical, with dimensions of approximately 2.4 mm width and 2 mm height above the substrate surface. Dilution in laser cladding may be defined as the ratio of the area of melted substrate to the sum of the area of melted substrate and area of material deposited as measured in a cross-section. The extent of substrate melting in this case corresponded to a dilution of $\sim 16\%$. EDAX analyses of areas of $160\text{ }\mu\text{m} \times 160\text{ }\mu\text{m}$ demonstrated that the clad layer was reasonably homogeneous; the composition over most of the cross-section was in the range 72 - $75\text{ mol } \%$ Al_2O_3 (25 - $28\text{ mol } \%$ SiO_2), which is greater than the alumina content ($60\text{ mol } \%$) of the precursor powder mixture (Fig. 5). Dilution may also be defined, assuming chemical homogeneity, as the ratio of the composition of the deposit minus that of

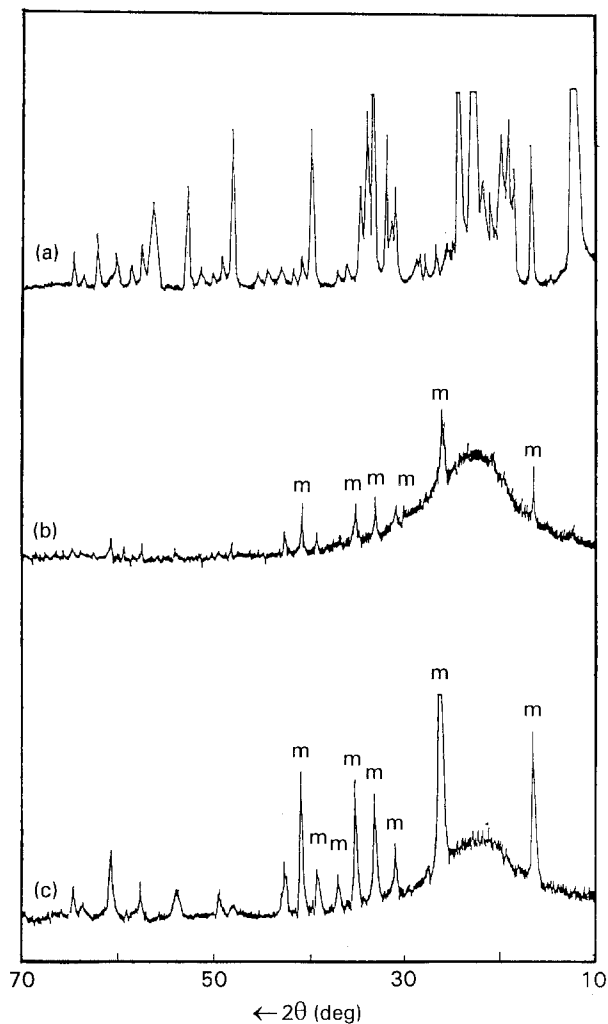


Figure 3 X-ray diffraction patterns for kaolin: (a) as-received powder, (b) pellet produced by laser processing, (c) pellet after heat treatment for 1 h at 1100 °C; m = mullite.

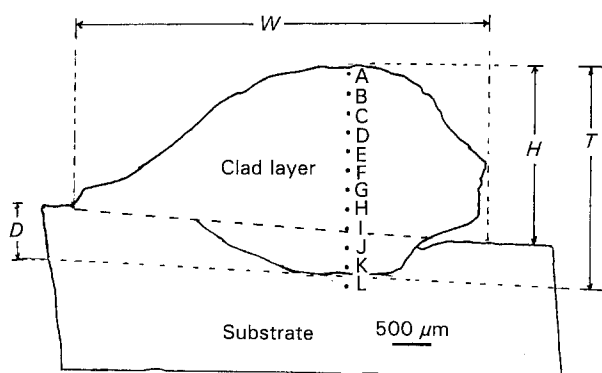


Figure 4 Diagram of cross-section of laser clad layer produced using SiO_2 -60 mol % Al_2O_3 mixture at a powder feed rate of 0.47 g s^{-1} , beam diameter 3 mm, traverse speed 5 mm s^{-1} and substrate preheat temperature $800 \text{ }^\circ\text{C}$; the letters denote the approximate areas where EDAX analyses were made.

the powder to that of the powder, and this gives a dilution of $\sim 22\%$, i.e. a slightly greater dilution than that calculated by the area method.

X-ray diffraction showed the presence of mullite and alumina and small amounts of silica and glass. Various morphologies were observed at different positions in the clad layer as shown by the scanning electron micrographs of Fig. 6. The structure of the

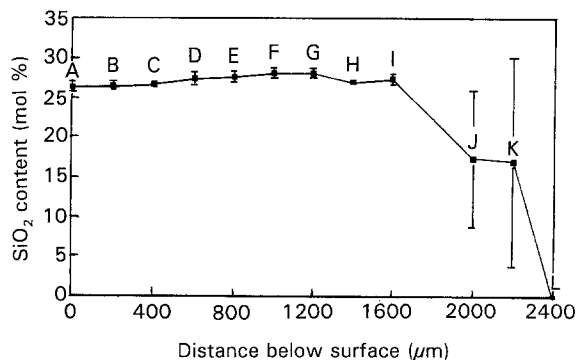


Figure 5 Composition distribution obtained by EDAX through the cross-section of the clad layer produced from precursor powder composition SiO_2 -60 mol % Al_2O_3 . The letters correspond to the positions marked in Fig. 4.

outer part of the layer was featureless ($\sim 30 \mu\text{m}$ thick in Fig. 6b). Regions of columnar, cellular/dendritic growth were observed in the upper and lower parts of the layer, with an indication of equiaxed dendrites in the central region. The cell/dendrite spacings were finer at the top as compared with the bottom of the clad layer. Some porosity and cracking was evident in the interface region.

Microhardness values taken from the top to the bottom of the clad layer showed some variation (1440 – 1780 kg mm^{-2}), presumably due to the changes in microstructure, and gave a mean of $1650 \pm 128 \text{ kg mm}^{-2}$. The microhardness of the clad is slightly less than that of the alumina substrate, which had a value of 1745 kg mm^{-2} . A lower value of 1372 kg mm^{-2} was obtained at the clad-substrate interface and this was attributed to the porosity present in this region.

The effect of traverse speed was investigated using the SiO_2 -60 mol % Al_2O_3 powder and the same processing conditions as previously, except that the speed ranged from 3.7 to 7.4 mm s^{-1} . In all cases alumina, mullite and a small amount of silica, which increased with increasing speed, were detected by XRD. The proportion of mullite present decreased with increasing traverse speed as shown by the plot of mullite/alumina intensity ratio against speed of Fig. 7. Microstructural examination revealed only partial melting of the powder at the faster speeds (6 and 7.4 mm s^{-1}).

Cladding experiments were also made with the SiO_2 - Al_2O_3 powder using the same processing conditions as before but at five different flow rates in the range 0.13 – 0.47 g s^{-1} . The X-ray results demonstrated that at low powder flow rates only alumina with a small amount of silica were present, whereas at the higher speeds (0.27 and 0.47 g s^{-1}) mullite had been formed (Table II). Sometimes small diffraction peaks which could have been assigned to tridymite were observed, but this information has not been included in the table.

The final cladding experiment carried out on the SiO_2 - Al_2O_3 powder was concerned with laser power density. In this experiment the 0.4 and 1 kW laser power levels were employed giving power densities of 44.4 and 111 W mm^{-2} , respectively. The lower power density resulted in partial melting and only alumina

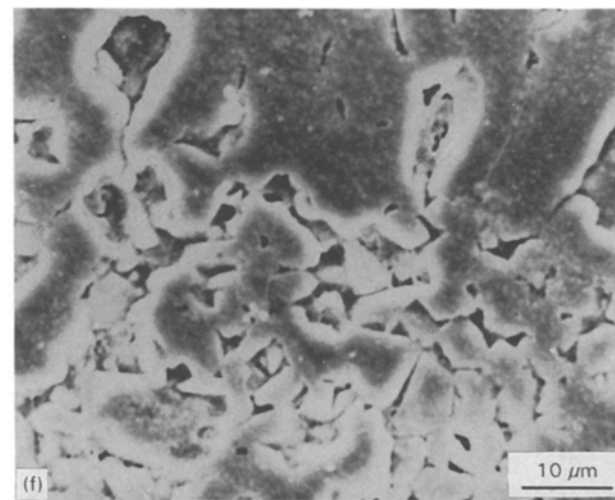
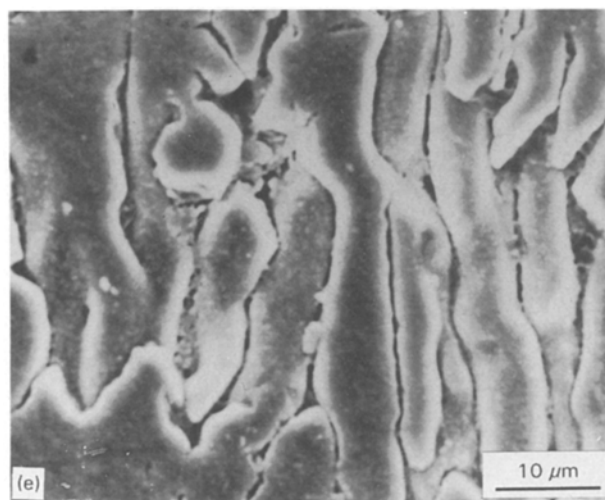
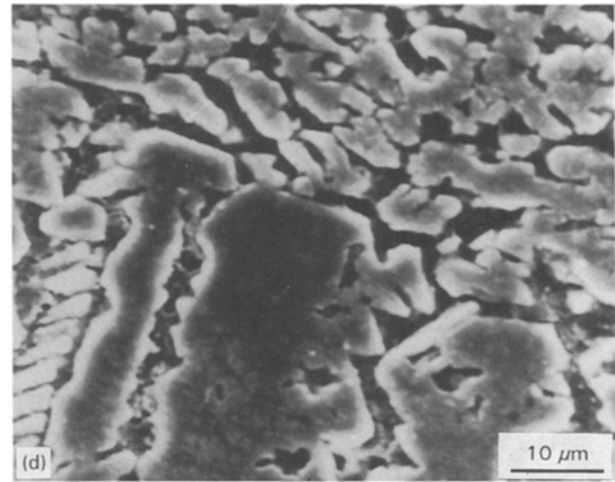
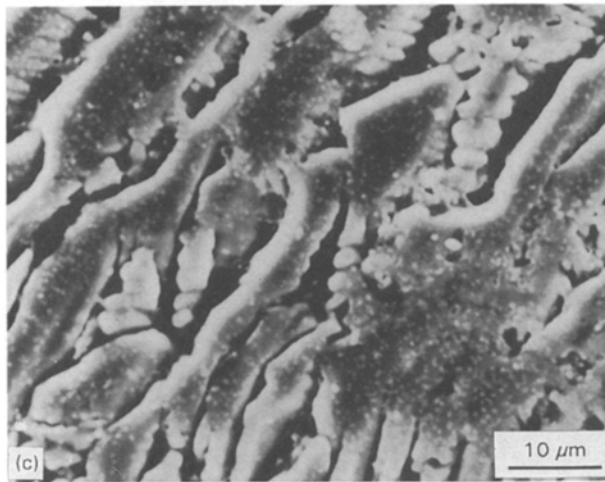
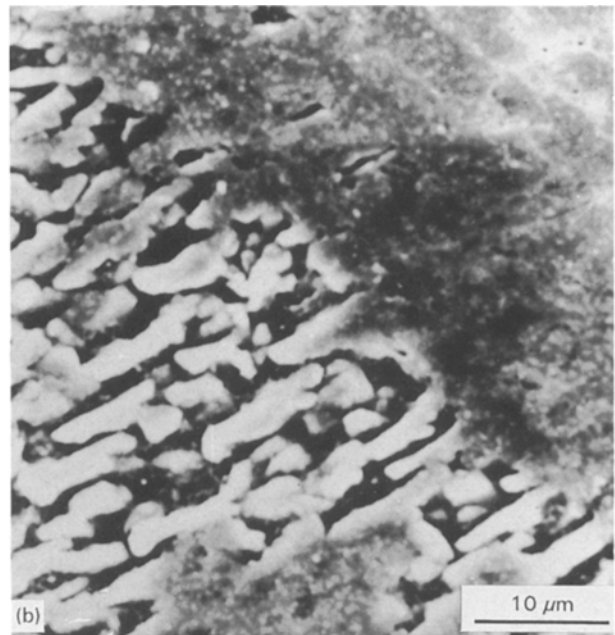
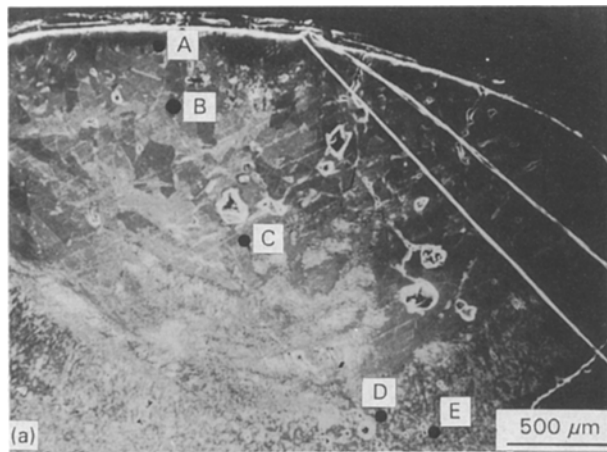


Figure 6 Microstructure of clad layer produced from SiO_2 -60 mol % Al_2O_3 mixture at a powder feed rate of 0.47 g s^{-1} , beam diameter 3 mm, traverse speed 5 mm s^{-1} and substrate preheat temperature $800 \text{ }^\circ\text{C}$. (a) Cross-section with positions of the following SEM micrographs marked by the letters A to E (diagonal lines in top right-hand corner are artefacts). (b) Position A: featureless surface layer and columnar structure. (c) Position B: columnar grains have become more dendritic. (d) Position C: equiaxed dendrites in the top half of the micrograph. (e) Position D: columnar structure above the clad-substrate interface. (f) Position E: porous region at the interface.

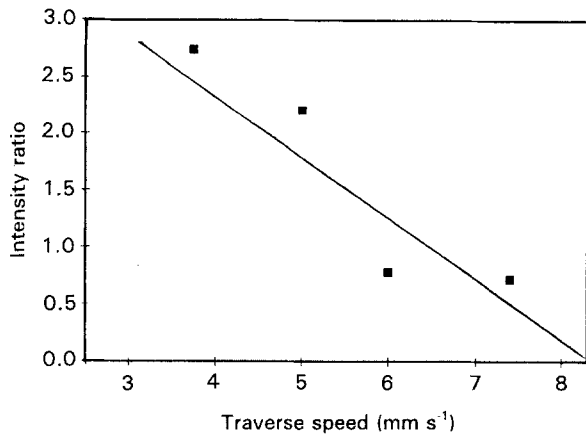


Figure 7 Plot of the ratio of the intensity of the X-ray diffraction peaks for mullite and alumina as a function of traverse speed when cladding using SiO_2 -60 mol % Al_2O_3 powder.

TABLE II Effect of powder flow rate on the phases present and their proportions (as determined by X-ray diffraction) in laser-processed clad layers produced from SiO_2 -60 mol % Al_2O_3

Powder flow rate (g s^{-1})	Phase proportion			
	Mullite	Alumina	Silica	Glass
0.13	None	Large	Small	None
0.16	None	Large	Small	None
0.20	None	Large	Small	None
0.27	Large	Medium	Small	Small
0.47	Large	Medium	Small	Small

and silica were detected by XRD. In contrast, as described earlier, at 1 kW (111 W mm^{-2}) full melting occurred and a substantial amount of mullite was formed.

In the clad layer produced using kaolin various growth morphologies, not unlike those described for the clad made from the SiO_2 - Al_2O_3 powder, were observed. For example, there was a thin featureless layer at the top of the clad; a dendritic structure was found in the upper regions of the clad below the featureless layer, whereas the structure in the centre of the clad was more equiaxed (Fig. 8). As for the powder mixture clads, the cell/dendrite spacings were finer at the top compared with the bottom of the clad layer. X-ray diffraction showed the dominant phase to be mullite. Unlike the pellets produced from kaolin, the porosity was not marked in the clad layer.

4. Discussion

4.1. Solidification

The structural observations in the various materials can be interpreted qualitatively in relation to the binary SiO_2 - Al_2O_3 phase diagram, bearing in mind that in the pellets the presence of significant amounts of glass in some cases shows that solidification was too rapid for the attainment of equilibrium. The use of a preheated substrate in the cladding experiments permitted equilibrium to more nearly be attained as shown by the absence, or the presence of only small amounts, of glass. Two important versions of the

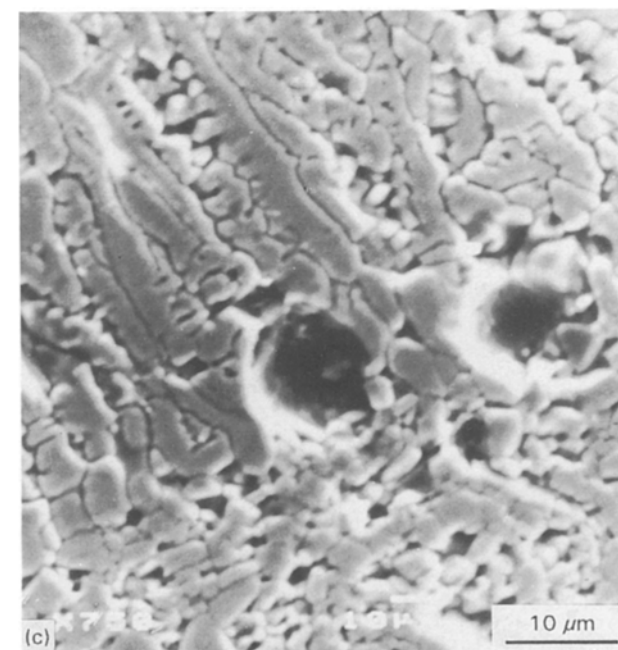
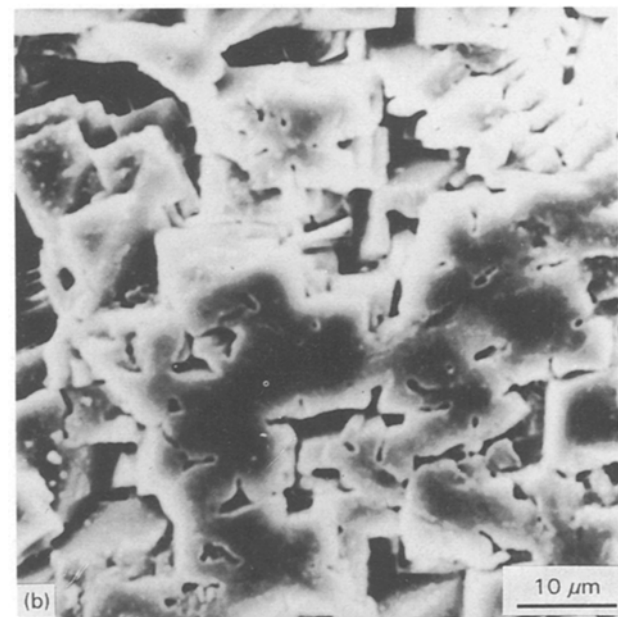
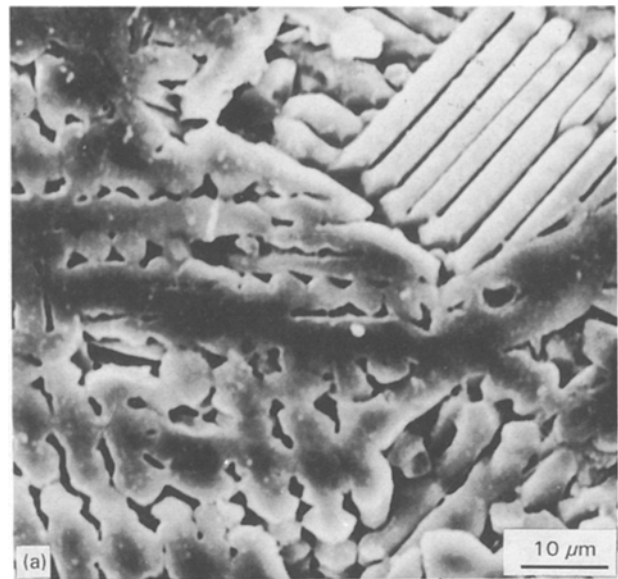


Figure 8 Typical microstructures found in the clad layer produced from kaolin: (a) a dendritic structure found in the upper regions; (b) a more equiaxed structure found in the centre of the clad layer; (c) columnar, dendritic growth from the clad-substrate interface.

phase diagram exist [14, 15] showing differences with respect to mullite formation. One [14] shows mullite melting congruently and forming eutectics with SiO_2 and Al_2O_3 respectively. The other [15] shows mullite forming by a peritectic reaction, namely $\text{liquid} + \text{Al}_2\text{O}_3 \rightarrow \text{mullite}$. The lamellar microstructural feature observed in the SiO_2 -60 mol % Al_2O_3 pellets is consistent with the formation of a mullite + Al_2O_3 eutectic, and consequently the former version of the phase diagram (Fig. 9) serves as an appropriate basis for discussing solidification. The SiO_2 -rich ends of both versions of the phase diagram are similar.

In the SiO_2 -60 mol % Al_2O_3 precursor pellets, in which mullite and Al_2O_3 were identified by XRD, the angular crystals were interpreted as primary mullite, and the lamellar structure as the Al_2O_3 + mullite eutectic. The phase diagram indicates that, at this composition, the structure at equilibrium should be essentially single-phase mullite. It is possible that loss of SiO_2 occurred by evaporation during the laser melting; silica loss would lead to eutectic formation. Little or no glass phase was expected at the high Al_2O_3 content and the small amount detected may be due to inhomogeneity of the pellet. The SiO_2 -70 mol % Al_2O_3 pellet also consisted mainly of mullite and alumina, which is consistent with phase diagram considerations, and an even smaller amount of glass. The very small amount of silica detected by XRD in this pellet was attributed to the unmelted particles of silica sticking to the surface of the pellets.

The main constituent of the pellet made from the most siliceous powder mixture (SiO_2 -40 mol % Al_2O_3) was mullite as predicted by the phase diagram. However, during solidification the silica-rich liquid resulting from the formation of the mullite crystals did not undergo the eutectic transformation but produced a glass. The kaolin precursor pellet consisted of substantial amounts of glass and only a little mullite, even though the alumina content was similar to that of the

previous pellet. This greater propensity for glass formation must be associated with the impurities in the kaolin. Evaporation of absorbed and combined water accounts for the large amount of porosity. Kaolin readily absorbs water on the surface which is lost on heating. Similarly the combined water is given off at temperatures greater than about 450 °C [16]. It should be noted that the porosity of the kaolin precursor clad layer was low, as preheating reduced the water content in a controlled manner prior to laser processing.

In the clad layer produced using kaolin the XRD evidence showing the presence of only mullite indicates that the final composition is very close to that of the compound. The slower cooling rate in cladding with the preheated substrates, as compared with pellet production, reduces any tendency to glass formation and the only glass present was probably associated with the thin, featureless upper layer.

The observations of cellular and dendritic crystals with columnar and equiaxed regions as a function of position in the clad layers produced either from the SiO_2 -60 mol % Al_2O_3 mixture or from kaolin are assumed to result from variations in thermal conditions during solidification and varying degrees of constitutional supercooling. The general pattern appears to indicate columnar growth upwards as a result of thermal conduction into the substrate, and also columnar growth downwards from the top and sides of the clad layer as a result of heat loss by radiation/convection. There is an indication of equiaxed crystal formation in the central regions of the clad, suggesting a relatively high level of constitutional supercooling.

The presence of a featureless surface layer, interpreted as a glassy phase, on some of the clads indicates that the cooling rate due to radiation/convection is significant. An estimate of the relative cooling rates in the clad layer near to the upper surface and close to the substrate was made from the secondary dendrite arm spacings in these regions. The relationship between cooling rate ϵ and secondary dendrite arm spacing λ has been deduced to be

$$\lambda = B\epsilon^{-n} \quad (1)$$

where B is a constant, dependent on the material, and n has a value of 0.33 [17]. Investigations on various metallic systems (e.g. [18]) have confirmed this relationship, although experimentally determined values of n are typically in the range 0.25 to 0.55. According to Equation 1, the ratio of the cooling rates (ϵ_u and ϵ_l) and spacings (λ_u and λ_l) in the upper and lower regions of the clad respectively is given by:

$$\frac{\epsilon_u}{\epsilon_l} = \left(\frac{\lambda_u}{\lambda_l} \right)^{-1/n}$$

The authors are not aware of values in the literature for n for ceramics and hence 0.33 was assumed. This value, together with the measured mean spacings of $\lambda_u \approx 3 \mu\text{m}$ and $\lambda_l \approx 7 \mu\text{m}$, gave 13 for the ratio of the cooling rates (ϵ_u/ϵ_l); this is consistent with the formation of a glass layer on the upper surface.

The difference in the dilutions when calculated by the areal method compared with the compositional

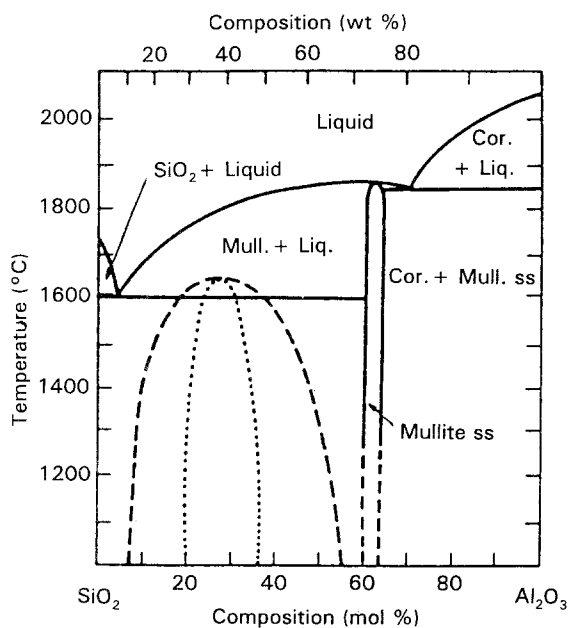


Figure 9 The SiO_2 - Al_2O_3 binary phase diagram according to Aramaki and Roy [14].

method, namely 16 and 22% respectively, can be accounted for by the loss of some silica by evaporation. A small silica loss would have a negligible effect on the areal dilution but would increase the dilution calculated from compositional changes.

4.2. Processing aspects

The previous section was concerned with the effect of composition on solidification and the resulting microstructure, but the processing conditions also play a major role. The dependence of the mullite content of the clad layers on traverse speed v (Fig. 7) may be discussed in terms of the interaction time t , which is defined as $t = d/v$ where d is the beam diameter. When the speed is low there is a long interaction time and a great deal of heat is transferred on to the specimen, so the formation of mullite is favoured as the cooling rate is not high. In contrast, at the higher speeds the interaction time is reduced and the energy absorbed may not be sufficient to melt the powder completely, thereby reducing the mullite content. Also the melt zone will be smaller the faster the traverse speed, leading to higher cooling rates and the tendency for glass formation.

A similar argument based on energy absorbed may be used to explain the effect of power density. At high power density (111 W mm^{-2}) mullite is formed due to complete melting and slow cooling, whereas low power density (44.4 W mm^{-2}) gives only partial melting followed by rapid cooling and hence no mullite.

Processing over a range of flow rates demonstrated that mullite formation was only found at the faster powder flow rates (Table II). It is considered that at the slow flow rates the limited amount of powder under the laser beam reaches a very high temperature, leading to silica loss. Also as the powder stream is thin the beam melts a considerable amount of the substrate which increases the dilution. Thus at slow flow rates the clad composition is more alumina-rich than the precursor powder mix, which accounts for the predominance of alumina in the clads. The structure of the clads produced at the faster flow rates ($> 0.27 \text{ g s}^{-1}$) was as described earlier for 0.47 g s^{-1} flow rate.

5. Summary

Pulsed laser beams applied to powder beds consisting of mixtures of ceramic constituents can be used to produce small (several millimetres diameter) pellets, approximately spherical in shape. Subject to appropriate control of process parameters, the technique offers a flexible approach to the study of rapid solidification of high melting-point ceramics over a wide compositional range. Also where glass formation occurs, the pellets can be used for the study of crystallization and of phase transformations on heating. Thus the technique is suited to phase diagram determination of ceramic systems.

All the pellets produced from alumina-silica powder mixtures in the range 40–70 mol % Al_2O_3 contained substantial amounts of mullite, but the glass content increased with decreasing Al_2O_3 in the mix-

ture. The notable features of the pellets produced from kaolin were the absence of mullite and the presence of a glassy phase with much porosity.

Cladding of ceramic alloy layers by laser processing, either by preplacing powder or continuous powder feed, presents considerable experimental difficulties if clad layers of uniform composition and structure, with minimal defects and of controlled dimensions, are required. Also preheating is required to reduce cracking in both the ceramic substrate and the clad layer.

The present work using a continuous feed of alumina-silica mixtures demonstrated that the structure of the clad layer depended on the composition of the feed mixture and the processing variables. For example, the mullite content of the clad decreased with increasing traverse speed and decreasing feed flow rate. With the processing conditions used in this study the cooling rate at the upper surface due to radiation/convection was significant. The structural observations in the various alloy compositions can be interpreted qualitatively in relation to the binary $\text{SiO}_2\text{-Al}_2\text{O}_3$ phase diagram, bearing in mind that in the pellets the presence of glassy phases shows that solidification was too rapid for the attainment of equilibrium; with the cladding process using heated substrates, equilibrium was more nearly approached and only small amounts of glass were observed.

References

1. H. MAROU and Y. ARATA, *J. Jap. Welding Soc.* **51** (1982) 182.
2. G. K. CHUI, *Amer. Ceram. Soc. Bull.* **54** (1975) 514.
3. J. A. RIDEALGH, R. D. RAWLINGS and D. R. F. WEST, *Mater. Sci. Tech.* **6** (1990) 395.
4. K. M. JASIM, R. D. RAWLINGS and D. R. F. WEST, *J. Mater. Sci.* **27** (1992) 3903.
5. *Idem.* *Surf. Coating Technol.* **53** (1992) 75.
6. *Idem.* in "Surface Engineering", Vol. III, edited by P. K. Datta and J. S. Gray Special Publication No. 128 (Royal Society of Chemistry, Cambridge, 1993) p. 50.
7. S. SAUNDERS, A. ANSARI and W. M. STEEN, "Laser Technology in Industry", SPIE **952** (1988) 514.
8. K. M. JASIM, R. D. RAWLINGS and D. R. F. WEST, *J. Mater. Sci.* **25** (1990) 4943.
9. K. M. JASIM, D. R. F. WEST, W. M. STEEN and R. D. RAWLINGS, in "Laser Materials Processing III", edited by J. Mazunder and K. N. Mukherjee (TMS, USA, 1989) p. 55.
10. R. CHAIM, A. H. HEUER and V. ARONOV, *J. Amer. Ceram. Soc.* **73** (1990) 1519.
11. R. D. RAWLINGS, Y. N. SHIEH, R. SWEENEY and D. R. F. WEST, in Proceedings of LASER-6, Sixth International Conference on High-Powered Laser Applications, Paris, 1990, edited by B. Mordike and A. B. Vannes (ITT International, Gournay-sur-Marne, France, 1990) p. 41.
12. M. IKEDA and S. MINETA, "Laser Advanced Material Processing" (Japanese Laser Processing Society, 1987).
13. V. M. WEERASINGHE, unpublished work, Imperial College (1989).
14. S. ARAMAKI and R. ROY, *J. Amer. Ceram. Soc.* **45** (1962) 229.
15. A. AKSAY and J. PASK, *ibid.* **58** (1975) 507.
16. F. H. NORTON, "Fine Ceramics Technology and Applications" (McGraw-Hill, New York, 1974) p. 240.
17. W. KURZ and D. J. FISHER, "Fundamentals of Solidification", (Trans Tech, Aedermannsdorf, Switzerland, 1986).
18. H. JONES, "Rapid Solidification of Metals and Alloys" (Institute of Metallurgists, London, 1982).

Received 1 March

and accepted 28 April 1994